Performance Evaluation of Backside Emitting O-Band Grating Couplers for 100μm-thick Silicon Photonics Interposers

Nivesh Mangal[*†], **Jeroen Missinne**[*], **Geert Van Steenberge**[*], **Joris Van Campenhout**[†],**and Bradley Snyder**[†]

[*] *Centre for Microsystems Technology, imec and Ghent University, Technologiepark-Zwijnaarde 126, Ghent B-9052, Belgium*

Email: nivesh.mangal@imec.be

[†] *imec, Kapeldreef 75, Heverlee B-3001, Belgium*

DOI: 10.1109/JPHOT.2009.XXXXXXX

Manuscript received - ; revised -. First published -. Current version published -.

Abstract: Most of the single-mode fiber-coupled grating couplers reported in the literature have been designed for upward directionality to perform wafer-scale testing of photonic integrated circuits. A coupler designed for downward directionality can help in achieving a face-up electro-optic integration scheme for chip-to-board coupling using 2.5D/3D silicon photonics interposers. We demonstrate for the first time the design analysis and coupling performance of TE-polarized O-band through-substrate (backside emitting) grating couplers that have been optimized to produce enhanced directionality in the downward direction into the bulk silicon substrate of a Si photonics chip. The chip substrate was thinned and polished to achieve a bulk silicon thickness of 100 μm. By the use of an optimized reflector and an optimal thickness of anti-reflection coating at the backside of the chip, a -2.3 dB and -1.7 dB fiber-to-grating coupling efficiency has been measured when coupled through-substrate to a single-mode and multimode fiber respectively. These gratings with downward directionality can help provide an efficient and alignment-tolerant interface for chip-to-chip or chip-to-board optical interconnects.

Index Terms: Silicon Photonics, Grating Couplers, Optical interconnects, Optical Interposers

1. Introduction

Optical interconnect based technology offers a promising solution to address the growing capacity requirement of datacenters [1]. In particular, CMOS-compatible silicon photonics can help provide both electronic and optical functionalities on a single chip leveraging the advantages of high index contrast, scaling, bandwidth, spectral density and power efficiency. In order to benefit from such advantages, it is desirable to have an on-chip optical interface that is not only highly efficient and alignment tolerant, but also exploits the CMOS-compatibility available with manufacturing processes developed for Si photonics over the years. In that respect, two coupling strategies have primarily been employed to route an optical signal off-chip to a package-level or a board-level optical interconnect: adiabatic optical coupling using an efficient taper design [2], [3] and a grating coupler based approach to couple to a fiber ribbon [4], [5] or to another grating for inter-chip coupling [6]. Grating couplers are a key passive optical component to perform wafer-scale testing of integrated photonic circuits. Although they are bandwidth-limited and more polarization-sensitive

TABLE I: Summary of O-band grating coupler performance (fiber in air) for upward directionality in recent years (t_{Si}: top silicon thickness, ed: etch depth, t_{BOX}: BOX thickness, CE: coupling efficiency).

Year	Reference	t_{Si}, ed, t_{BOX} (nm)	Description	3dB BW	Peak CE(dB)
2011	[8]	$400, 200, 1000$	Single-etch uniform	58	-3
2014	[9]	$220, (60, 130), 2000$	Dual-etch apodized	50	-2
2016	[10]	$220, 220, 2000$	Sub-wavelength	–	-2.5
2017	[11]	$220, 220, 2000$	Sub-wavelength	40	-3.8
2017	[12]	$340, 140, 2000$	Tilted membrane	> 70	-2.4
2017	[13]	$200, 35, 2972$	Folded Shallow	–	-2.23
2017	[14]	$310, 140, 720$	Apodized	35	-2.2

compared to edge-couplers, they provide advantages in terms of wafer-scale accessibility and die-level planarized packaging solutions. Ever since the demonstration of on-chip gratings for fiber-coupling [7], there has been a lot of focus to push the device performance envelope with respect to coupling efficiency, bandwidth and polarization diversity. Most of the research efforts in this domain have been in the spectrum of C-band wavelengths for telecom-based long-reach applications due to the low absorption loss of silica in an optical fiber and the relaxed patterning requirements during fabrication of grating features. In the recent times, a need to address high-speed short-reach interconnections in server based applications of modern data-centers has resulted in an increased effort to develop similar high performance grating designs in the O-band (1310 nm primary wavelength) due to the reduced chromatic dispersion in an optical fiber in this band. Table I outlines the design methodology and performance of some of the recent demonstration of such gratings. The optimization of these gratings for upward directionality has been done by tuning the total silicon thickness, etch depth and performing apodization of the grating or by operating in the subwavelength regime.

It is well-understood that the off-chip optical coupling for chip-to-package and chip-to-board communication requires a strategy that not only benefits from the CMOS-based wafer-scale platforms available for silicon photonics, but also helps to minimize the cost incurred in packaging and assembly of a 2.5D/3D optical interposer. In contrast to the approaches demonstrated before [2], [5], [15], a through-substrate coupling interface provides the benefit of bonding a silicon photonics chip face-up on a package substrate such that the device-side of the chip remains accessible for die stacking, and there is no need to develop space for fiber-array placement from the topside, and can provide an alternative to flip-chip photonic packaging (Fig. 1). Such an approach can then be utilized to assemble memory and logic dies with the help of TSVs and microbumps on the top of a silicon photonic interposer in a 3D electro-optic integration scheme [16]–[19]. In this context, an O-band grating coupler designed for downward directionality is required. To address this problem, we demonstrate the design and performance of the O-band grating couplers that help in achieving optimized directionality in the direction of the substrate. Although there have been only a few demonstrations in the past for downward directionality [20],

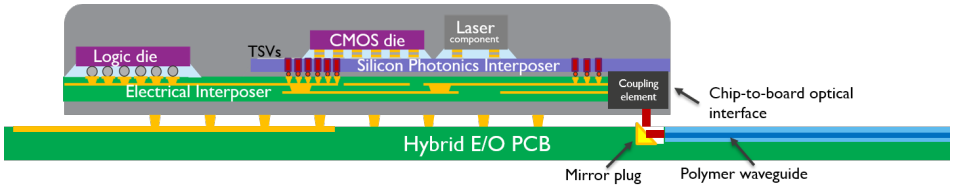

Fig. 1: Overview of 2.5D/3D integration of Silicon Photonics for chip-to-board coupling.

[21], they have been fabricated in a monolithic 45nm CMOS SOI process platform used for defining transistors (and hence, different thickness of top silicon $<$ 100 nm); gratings optimized for a center wavelength of 1200 nm, measurements performed by removing the bulk silicon substrate and an unconventional fiber-to-grating coupling angle of 19° was used. In contrast, we report the results for gratings that use a metal reflector, defined in a standard 220 nm top silicon of 200 mm wafer-scale SOI platform developed at imec, with only partial removal of silicon handle substrate and a standard fiber-coupling angle of 10°. The topside reflector approach is more practical and compatible with the back-end of the line (BEOL) processing used in a typical CMOS process flow, when compared to depositing the reflector between the BOX-Si interface as has been already demonstrated for high upward directionality [22]–[24]. For the gratings with metal reflector deposited over the top oxide, the downward directed beam propagates in the bulk silicon substrate that has been thinned to 100 μm thickness to match the standard thickness of TSVs used for silicon interposers. The fiber-to-waveguide coupling efficiency has been measured using both single-mode and multimode fibers. In this paper, firstly, the device design simulations are analyzed. Then, the fabrication and measurement methodology of the grating couplers are explained briefly. Finally, a comprehensive study on the experimental results is done to underline the utility of such devices for 2.5D/3D silicon photonics interposers [18], [25].

2. Grating coupler with a metal reflector: Design

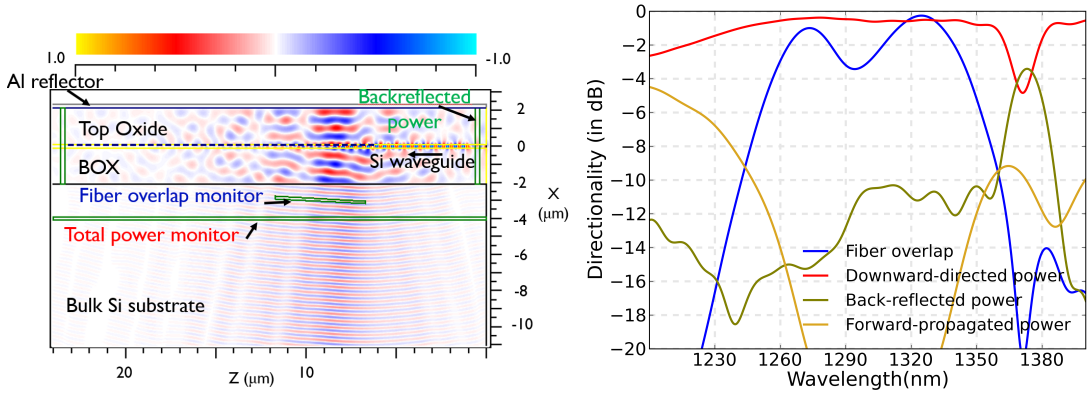

(a) (b)

Fig. 2: a) 2D Field plot of a grating coupler FDTD simulation and b) Directionality plot of the grating coupler spectrum highlighting the fact that about 90% of the power is diffracted in the downward direction across the central O-band, while roughly 10% gets backreflected in the counter-propagating direction in the top and bottom oxide and silicon waveguide combined. (The color code of the power monitor labels in (a) correspond to the labels of the plot in (b)).

A grating coupler with a uniform period diffracts the incoming optical signal in a particular direction according to the following phase matching condition:

$$\Lambda = \frac{m\lambda}{n_{\text{eff}} - n_{\text{clad}} \sin\theta} \tag{1}$$

where Λ is the grating period, λ is the free-space optical wavelength in vacuum, n_{eff} is the effective index of the eigen mode of the grating, n_{clad} is the cladding index and, θ is the angle of diffraction of the optical signal. The grating is typically slightly detuned to avoid second-order reflections at the waveguide-grating groove interface. The coupling efficiency of a grating coupler is defined by the directionality of the diffracted power from the grating and the mode overlap between the diffracted

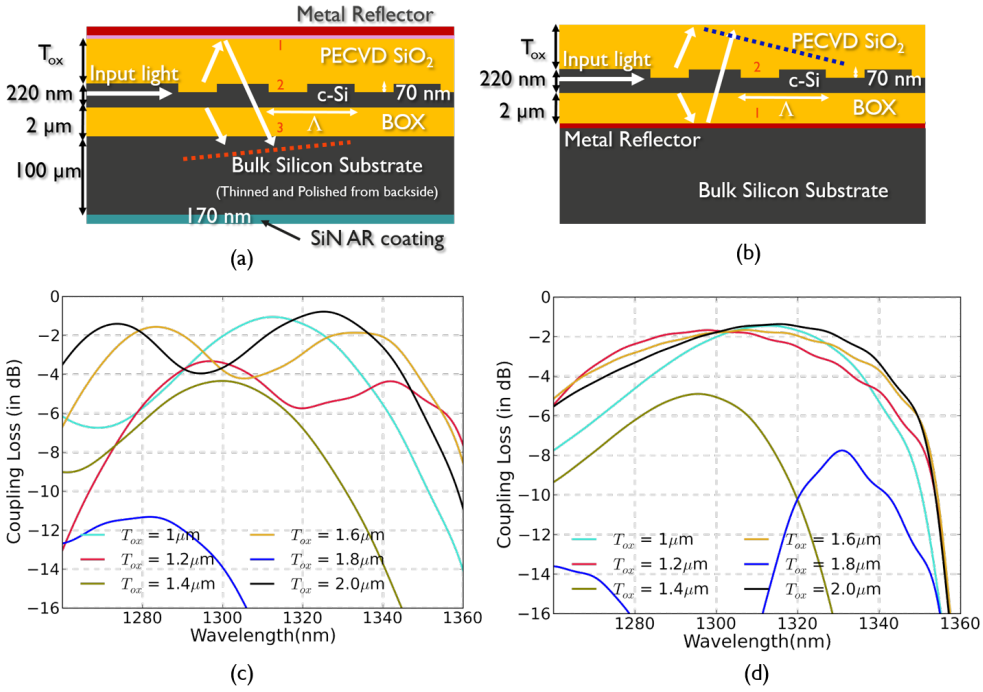

Fig. 3: Comparison of uniform period TE polarization SOI grating couplers with a metal reflector for (a,c) downward and (b,d) upward directionality. The effect of oxide thickness on fiber-to-grating coupling efficiency spectrum is shown with the help of 2D-FDTD simulations for both the cases of directionality. The numbers(in red) inside the figures (a) & (b) indicate the interfaces where an optical wave experiences a perturbation. While the fiber monitor for (a,c) was kept in silicon near BOX-silicon interface (orange dotted line), the same was kept in top oxide for (b,d) (blue dotted line). Grating parameters: Λ = 490 nm, Fill-Factor = 0.5, Etch depth = 70 nm, Top silicon thickness = 220 nm, Bulk silicon substrate thickness = 100 μm, T_{ox} = oxide thickness that is optimized for a given directionality.

field profile from the grating and the Gaussian-like optical fiber mode. One approach to improve the directionality of these couplers in the upward direction has been to deposit a metal reflector between the BOX and the bulk silicon substrate [22]–[24]. In order to enhance the directionality in the downward direction, a metal reflector on the oxide cladding was deposited above the diffraction grating. By exploiting constructive interference between the downward diffracted optical signal from the grating and the upward diffracted signal reflected downwards from the metal reflector for a particular oxide thickness, a net downward directionality is achieved (Fig. 3a,c).

The thickness of the top oxide required for constructive interference is given by:

$$t_{\mathrm{ox}} = \frac{\cos\theta_{\mathrm{ox}}}{n_{ox}} \cdot \left(\frac{m\lambda}{2} - \frac{t_{\mathrm{Si}} . n_{\mathrm{avg}}}{\cos\theta_{\mathrm{avg}}} \right) \tag{2}$$

where t_{ox} is the top oxide thickness, t_{Si} is the thickness of the etched silicon (70 nm in this case), m is an integer, n_{ox} is the refractive index of the top oxide, n_{avg} is the average of the refractive index of the etched grating, θ_{ox} the angle of the diffracted beam in oxide and θ_{avg} the corresponding angle of the diffracted beam in the average index material of the grating. The thickness of the etched grating and its refractive index is taken into account to include the additional phase that the diffracted and reflected beam would acquire before constructively interfering with the downward diffracted beam. Also, in order to accurately optimize the thickness of top oxide for constructive

interference, 2D FDTD simulations were performed (see Fig. 2). The grating couplers for downward directionality were designed for parameters corresponding to a standard SOI wafer with a 220 nm thick silicon waveguide layer and a 2 μm thick buried oxide layer (BOX). The period and etch depth of the grating was kept at 490 nm and 70 nm respectively for TE polarization in the simulations corresponding to a 10° angle of the fiber in air and hence, after refraction at the air/silicon interface, a 2.81° angle of the overlap monitor defined in the bulk silicon substrate near to the BOX-silicon interface in the simulations (as shown by the dotted line in Fig. 3a). The placement of the fiber-coupling overlap monitor near this interface enabled the minimization of overall computation time in FDTD simulations. From paraxial Gaussian beam propagation relations, it can be estimated that a Gaussian-like mode from an optical fiber expands from 9.2 μm to only 10.4 μm in a 100 μm bulk silicon medium with a negligible absorption loss. The coupling loss due to mode size mismatch was calculated to be 0.32 dB. We revisit this assumption in Section 4.2 later while comparing the experimental results. In Fig. 3, a comparison of the wavelength dependence of the grating for both the cases of directionality has been made by changing the oxide thickness(top oxide for downward directionality (a,c) and BOX for upward directionality (b,d)). The following observations are made here:

i) One of the possible optimal thicknesses of top oxide required for constructive interference in the downward directionality at a fiber angle of 10° in air was calculated to be 2 μm, as can be roughly predicted (2033.5 nm) by Eq.(2). The peak coupling efficiency near the BOX-silicon interface was estimated to be -1 dB with a 45 nm 3 dB bandwidth [26].

ii) An uneven dual-peak shape of the spectrum appears in the case of downward directionality grating. This is due to the presence of an additional reflective interface between the BOX and the Si substrate and will be discussed further in section 4. As the oxide thickness changes, the effective optical path length between the two reflected components from interface 1 and 3 changes accordingly, resulting in a change in the relative levels of the two peak spectrum. In the case of the grating couplers with upward directionality however, the top oxide merely acts as an index matching medium between the optical fiber and the grating and hence, the two-peak shape of the spectrum is absent there.

iii) Also, as shown in Fig. 2b, around 10% of power(both from the reflector and the BOX-Si interface) gets backreflected into the oxide cladding and silicon waveguide resulting in 90% net downward directionality into the substrate. This case gets exemplified at a wavelength of around 1370 nm where a sharp drop in the directionality can be observed due to a phase matching of the two reflected components with the grating in the counter-propagating direction.

3. Fabrication and Measurement

Test chips with various focused grating coupler designs were fabricated in imec's 200 mm silicon photonics platform. The top oxide thickness on the wafers was varied by a margin of $\pm$50 nm to inspect its sensitivity on the measured coupling efficiency. The dies taken from different wafers were then further custom-processed to have 5 nm Ti + 200 nm Al metal reflectors deposited on top of the gratings. These chips were then bonded onto a glass carrier with wax that was subsequently used to perform lapping and polishing of the dies from the backside [27]; starting with a silicon thickness of 650 μm to a final value of 100 μm. After releasing them from the glass carrier with the help of a solvent, a 170 nm PECVD SiN anti-reflective coating was deposited on the polished substrate-side of these chips.

The dies were then flip-mounted onto a vacuum chuck so that fibers oriented at a 10° angle could be used to couple through the silicon substrate in and out of the gratings from the backside of the chip. The grating structures could be located with the help of an IR camera that allows to see through the polished bulk SOI substrate. The measurement setup included a O-band fiber-coupled

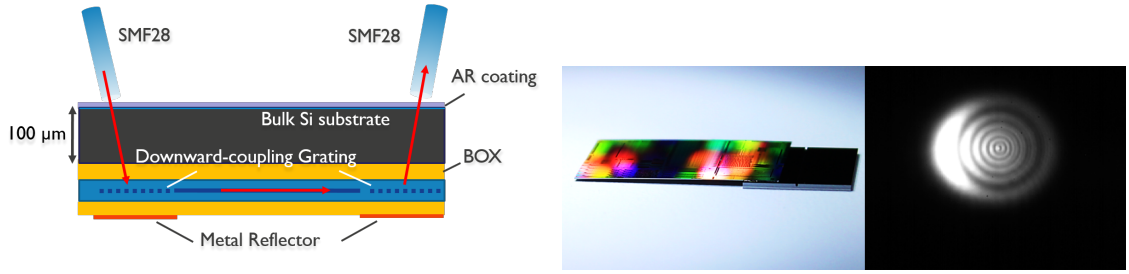

(a) (b)

Fig. 4: a) Measurement methodology of downward emitting grating couplers with single-mode fibers oriented 10° with respect to vertical, from the substrate-side of the chip and b) silicon photonics chip post thinning (left) with an IR beam profile in the far-field emitted by the grating coupler through the substrate of the polished chip (right).

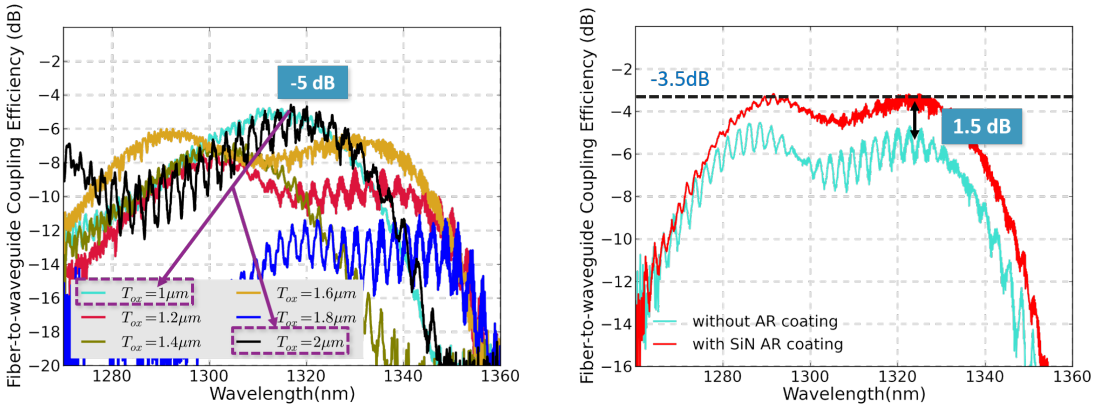

(a) (b)

Fig. 5: a) The effect of the variation of top oxide thickness on the measured fiber-to-waveguide coupling efficiency of the downward emitting grating coupler (without AR coating). (b) A 1.5 dB improvement in the coupling efficiency of the grating couplers occurs after the application of SiN anti-phase coating to counter the Fresnel reflections at the substrate side of the chip. (All the samples measured in these measurements had a 5 nm Ti adhesion layer between Al metal reflector and oxide (refer Section 4.1 for further discussion).)

broadband SLD source that was connected to a circulator followed by a polarization controller that was then connected to the input fiber pigtail. Also, the output fiber pigtail was connected to a power splitter that was connected to a power meter and optical spectrum analyzer respectively to aid in the simultaneous alignment of the fibers and recording of the spectrum thereafter. The fiber-to-waveguide coupling efficiency was calculated by subtracting the setup reference loss and waveguide loss from the measured spectrum and then dividing the obtained result by half.

4. Results and Discussion

In order to validate the results obtained from the 2D FDTD model corresponding to the variation in oxide thickness (discussed in Section 2), different chips comprising of gratings with a 490 nm period and 50% fill factor were processed to obtain different top oxide thicknesses before the deposition of the Ti+Al metal layer. A variation in steps of 200 nm in oxide thickness was done from 1 μm to 2 μm. Here, the chips were not coated with any anti-reflective coating from the polished

backside. It can be seen from Fig. 5a that the wavelength dependence of fiber-to-grating coupling efficiency is similar to what was derived from the FDTD simulations (Fig. 3c). A peak coupling efficiency of -5 dB was obtained for an oxide thickness of 2 μm. The free spectral range(FSR) of the ripples in the spectrum caused by Fresnel reflections from the silicon-air interface correspond approximately to 100 μm thickness of silicon (t_{Si}), given by the relation, $\mathrm{FSR} = \lambda^2/(2n_g t_{\mathrm{Si}} \cos\theta)$, where n_g is the group index of the optical wave propagating in silicon. After the deposition of 170 nm thick anti-reflective SiN coating [28], a reduction in the ripple amplitude and an improvement in the coupling efficiency by 1.5 dB margin was obtained as shown in Fig.5b.

4.1. Sensitivity of coupling efficiency on Ti adhesion layer below the Al reflector

In a typical CMOS process flow, it is usual to have TiN, TaN or Ti as an adhesion layer for the deposition of Aluminium(Al) or Tungsten(W) on silicon oxide [29]. In the recent demonstrations of grating couplers where metal reflectors have been employed to increase the upward directionality of the gratings, some of the research groups used Au as a reflector with BCB or Cr as an interfacial layer, where Au is a CMOS-incompatible material [30]. Also, some groups reported results using Aluminium (Al) as a reflector with an interfacial layer(Ti) [31], [32] or no interfacial layer at all [22], but didn't demonstrate any impact of the interfacial/adhesion layer thickness on the coupling efficiency measurements. We show that the thickness of the adhesion layer(Ti) between the Al reflector and planarized oxide has an impact on the overall reflectivity and hence, the coupling efficiency. In order to investigate this, measurements on three samples with different thicknesses of titanium between the Al reflector and top oxide were performed. From Fig. 6a, it is apparent that an improvement in coupling efficiency of the grating results from the case when the Al reflector was directly deposited on the silicon oxide clad above the grating. This can be verified from the transmittance value of titanium - 0.815 for 5 nm Ti and 0.92 for 2 nm Ti [33] and the reflectivity measurements shown by Fig. 6b. These measurements were done by collecting the reflected signal from a circulator port when an optical fiber was brought close to the titanium film of 2 nm and 5 nm thickness. Index-matching (NOA61) was used to ensure that fiber-air Fresnel reflections are minimized and only the true reflected signal is recorded. The measurements were then normalized with respect to the measurement done with a bare Al reflector. The proportional increase in loss with the increase in thickness of Ti confirms its contribution in reduction of the coupling efficiency of the gratings.

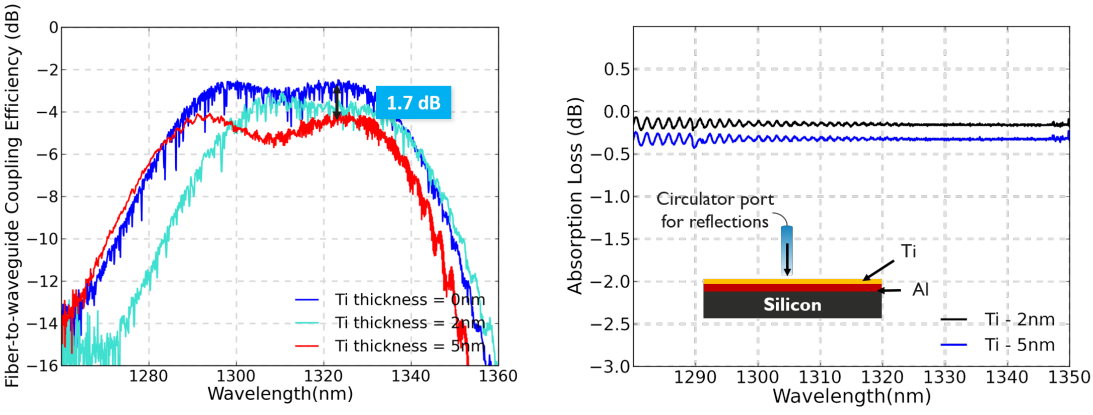

(a) (b)

Fig. 6: (a) Reduction in the thickness of adhesion layer between the grating and metal reflector results in a net reduction of absorption and an improvement in the overall fiber-to-grating coupling efficiency. (b) Absorption spectrum of different film thickness of Ti indicates a proportional increase in absorption with increasing thickness of Ti.

It should also be noticed that a direct deposition of Al on the top of silicon oxide results in a few nanometers thick layer formation of Al_2O_3 dielectric that can enhance adhesion, but isn't favored in a flow due to reduction in conductivity of the metal interconnects placed elsewhere on the same layer. Also, Al_2O_3 is a partially absorbing medium in the near-IR wavelength domain. This explains why there isn't any significant improvement in the coupling efficiency of a grating coupler when one compares the results of the gratings with pure Al reflector and a 2nm Ti+Al reflector (Fig. 6a).

4.2. Sensitivity of coupling efficiency on top oxide thickness

As explained earlier in Section 2, for the case of gratings with metal reflectors on top oxide for downward directionality, there are three distinct interfaces that contribute to the change in the phase of the diffracted beam - grating-oxide, oxide-reflector and BOX-silicon interface. This implies that a variation in the thickness of the top oxide cladding and the BOX can have an impact on the resultant coupling efficiency. As an example, for a 2 μm BOX thickness, it has been reported earlier that a $\pm$50 nm wafer-to-wafer variation in oxide thickness is possible [34]. The problem is compounded further when one takes into account the variability of top oxide thickness post-planarization. A minor contribution to lower the coupling efficiency can also be due to a variation in the thickness of the chip post-lapping and polishing. Fig. 7(a) shows the sensitivity of the coupling efficiency to a $\pm$50 nm variation in the top-oxide thickness deposited on different wafers. The following observations are made here:

i) The peak coupling efficiency drops by 0.5 dB with a change in oxide thickness of 50 nm. The presence of high frequency ripples in most of these measurements is an outcome of etch-density related effect.

ii) The two-peak shape of the spectrum varies with the change in top oxide thickness, as the optical path length for constructive interference shifts accordingly;

iii) The overall spectrum experiences a red shift as the top oxide thickness increases.

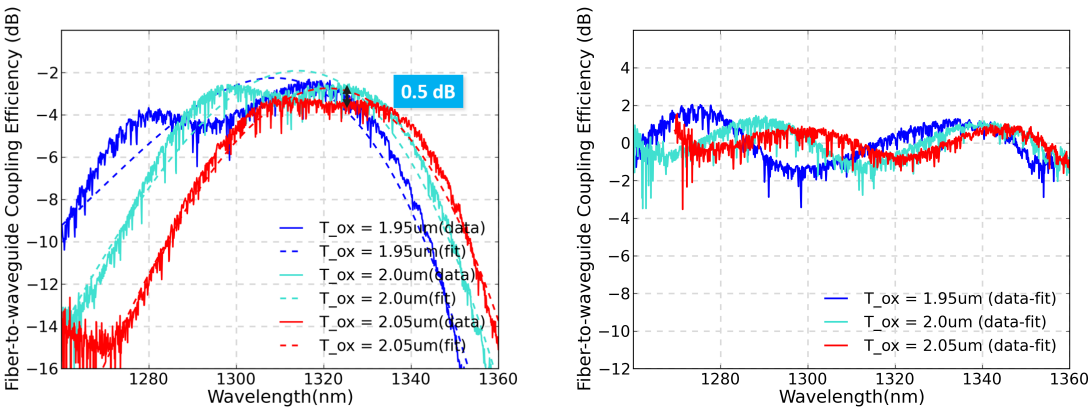

(a) (b)

Fig. 7: (a) A variation in oxide thickness of $\pm$50 nm results in a marginal drop of coupling efficiency with a change in the relative amplitude of the two-peak spectrum and a shift in the peak wavelength. The measured data is fitted with a 4th degree polynomial fit. (b) On subtracting the fit with the measured data, it can be seen that the period of the ripples decrease with increase in oxide thickness indicating an increase in path length of the beam between the two reflective interfaces and hence, their contribution to the formation of two-peak spectrum.

In order to understand the impact of oxide thickness on coupling efficiency further, a 4th degree polynomial fit was applied to the measured spectrum. When the experimental data was subtracted

from the fitted data (Fig. 7b), it was observed that the period of the ripples decrease with an increase in oxide thickness. This indicates a relative increase in the path length of the beam between the grating and the metal reflector and hence, its contribution to the different levels of the two-peak spectrum. Also, a difference of more than 1 dB in the measured coupling efficiency compared to that in the simulations can be attributed to the following reasons: a) A grating coupler with a uniform period radiates an exponentially decaying diffracted beam profile, that is usually matched with a fiber mode placed in close proximity to the grating. The same was done in the simulations by placing an overlap monitor in bulk silicon near the BOX-silicon interface as shown in Section 2. However, the actual coupling efficiency to the fiber has been measured roughly at a distance of 100 μm away from that interface. This results in additional loss apart from the mode mismatch assumption considered earlier as the beam propagation mechanism of an exponentially radiating profile in a bulk medium can not be assumed to be driven completely by Gaussian beam propagation relations, resulting in lowering of the overall coupling efficiency. b) Although the bulk silicon substrate of an SOI wafer is mostly transparent in the IR wavelength region of interest, dopant-induced scattering effects might contribute to some loss as well.

4.3. Coupling Efficiency with Multimode Fiber

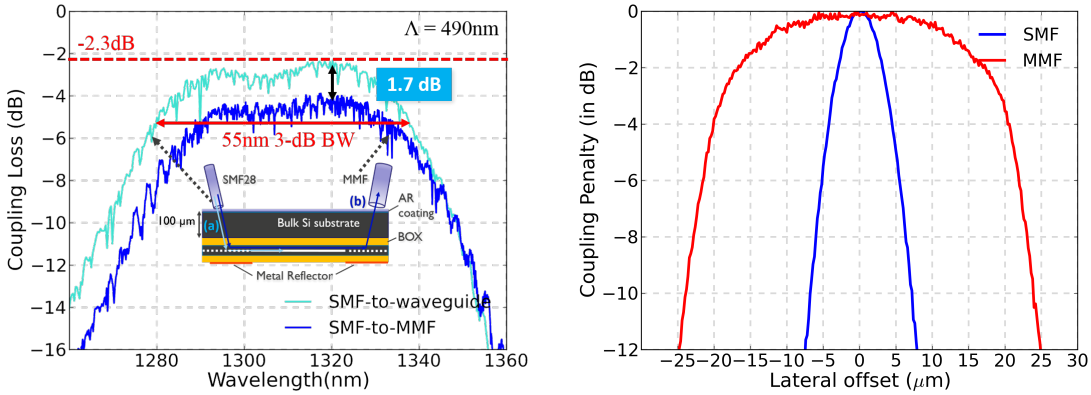

(a) (b)

Fig. 8: (a) A 1.7 dB loss from the downward-emitting grating would occur if it were to be coupled to a 50 μm core diameter multimode fiber. (b) An alignment tolerance scan comparison of single-mode fiber and multimode fiber coupled to a downward-emitting grating coupler.

In the case of coupling to a multimode fiber, the mode profile emitted from the grating is less critical as long as it couples well into a larger core diameter of the multimode fiber at a suitable angle. A separate set of measurements were conducted with a 0.2 NA 50 μm core diameter graded-index multimode fiber in order to assess the amount of power the grating can transmit if it were to couple into a multimode waveguide for an interposer application. This was done by aligning the multimode fiber at the output grating side, keeping the input launch conditions from the single-mode fiber fixed. A comparison of lateral alignment tolerance made with a single-mode fiber and multimode fiber on the grating coupler is shown in Fig. 8b. The SMF-to-MMF spectrum as depicted in Fig. 8a indicates the combined loss of single-mode fiber to the through-substrate input grating and the output grating through-substrate to the multimode fiber. The waveguide loss was subtracted from this spectrum. On comparing it to the coupling efficiency of a single-mode fiber to a grating coupler, it can be seen that a 1.7 dB loss would occur from an output grating coupler, if it were to be coupled into a 50 μm core diameter multimode waveguide. The results presented here give an idea about the expected max. coupling efficiency and alignment tolerance for coupling from the described downward emitting grating coupler on a Si photonics interposer

to on-package or on-board multimode optical interconnect [16], [25].

The results presented in the above sections hold a key practical relevance from the standpoint of understanding oxide-reflector interface, oxide-thickness tolerance that can arise out of wafer-scale manufacturability and fiber coupling efficiency with no removal of silicon handle substrate contrary to what has been done in the past [20], to counter a strong oxide-silicon reflective interface. These results also look promising when compared to O-band grating coupler performance for upward directionality as summarized in Table I.

5. Conclusion

We have demonstrated the results on O-band through-substrate (backside emitting) grating couplers optimized for downward directionality on photonic chips with 100μm thick bulk silicon substrate. The gratings show a peak coupling efficiency of -2.3 dB with a 3-dB bandwidth of 55 nm. A sensitivity analysis of grating coupler efficiency with respect to top oxide thickness and Ti adhesion layer was done. A 1.5 dB drop in coupling efficiency with the addition of 5 nm thick Ti as adhesion layer between Al reflector and top oxide was measured. A 0.5 dB sensitivity in coupling efficiency to a $\pm$50 nm variation in top oxide thickness was determined as well. In addition, when coupled to a multimode fiber, a -1.7 dB coupling efficiency is obtained which is important from the perspective of coupling from a Si-photonics interposer to multimode waveguide based optical interconnects. We believe that the overall performance of these couplers can be improved further by apodizing the gratings. Lastly, grating couplers with a downward directionality find applications not only in inter-chip coupling, but also in on-chip sensing and spectroscopy as they provide an alternate route to guide the resultant optical output other than in the conventional direction, albeit at the expense of some additional backside silicon processing.

Acknowledgments

The primary author would like to thank Muhammad Muneeb and Steven Verstuyft for providing assistance in the deposition of thin-film metal reflectors and anti-reflective nitride coating at intec Photonics, Ghent University. Also, the authors would like to acknowledge assistance from Sadhish Balakrishnan, Guy Lepage and Peter Verheyen, imec in providing chips from relevant wafers with the required oxide thickness. This work has been carried out as part of imec's industry affiliation program on Optical I/O.

References

[1] M. A. Taubenblatt, "Optical interconnects for high-performance computing," *Journal of Lightwave Technology*, vol. 30, no. 4, pp. 448–457, 2012.

[2] T. Barwicz, Y. Taira, T. W. Lichoulas, N. Boyer, Y. Martin, H. Numata, J.-W. Nah, S. Takenobu, A. Janta-Polczynski, E. L. Kimbrell, R. Leidy, M. H. Khater, S. Kamlapurkar, S. Engelmann, Y. A. Vlasov, and P. Fortier, "A novel approach to photonic packaging leveraging existing high-throughput microelectronic facilities," *IEEE Journal of Selected Topics in Quantum Electronics*, vol. 22, no. 6, pp. 455–466, 2016.

[3] R. Dangel, A. La Porta, D. Jubin, F. Horst, N. Meier, M. Seifried, and B. J. Offrein, "Polymer waveguides enabling scalable low-loss adiabatic optical coupling for silicon photonics," *IEEE Journal of Selected Topics in Quantum Electronics*, vol. 24, no. 4, pp. 1–11, 2018.

[4] K. Yashiki, T. Uemura, M. Kurihara, Y. Suzuki, M. Tokushima, Y. Hagihara, and K. Kurata, "25-Gbps/ch error-free operation over 300-m mmf of low-power-consumption silicon-photonics-based chip-scale optical I/O cores," *IEICE Transactions on Electronics*, vol. 99, no. 2, pp. 148–156, 2016.

[5] K. Kurata, Y. Suzuki, M. Tokushima, and K. Takemura, "Silicon photonics for multi-mode transmission," in *Optical Interconnects for Data Centers*. Elsevier, 2017, pp. 197–222.

[6] Y. Zhang, D. Kwong, X. Xu, A. Hosseini, S. Y. Yang, J. A. Rogers, and R. T. Chen, "On-chip intra-and inter-layer grating couplers for three-dimensional integration of silicon photonics," *Applied Physics Letters*, vol. 102, no. 21, p. 211109, 2013.

[7] D. Taillaert, W. Bogaerts, P. Bienstman, T. F. Krauss, P. Van Daele, I. Moerman, S. Verstuyft, K. De Mesel, and R. Baets, "An out-of-plane grating coupler for efficient butt-coupling between compact planar waveguides and single-mode fibers," *IEEE Journal of Quantum Electronics*, vol. 38, no. 7, pp. 949–955, 2002.

[8] N. Na, H. Frish, I.-W. Hsieh, O. Harel, R. George, A. Barkai, and H. Rong, "Efficient broadband silicon-on-insulator grating coupler with low backreflection," *Optics letters*, vol. 36, no. 11, pp. 2101–2103, 2011.

[9] R. Shi, H. Guan, A. Novack, M. Streshinsky, A. E.-J. Lim, G.-Q. Lo, T. Baehr-Jones, and M. Hochberg, "High-efficiency grating couplers near 1310 nm fabricated by 248-nm DUV lithography," *IEEE Photon. Technol. Lett.*, vol. 26, no. 15, pp. 1569–1572, 2014.

[10] D. Benedikovic, C. Alonso-Ramos, P. Cheben, J. H. Schmid, S. Wang, R. Halir, A. Ortega-Moñux, D.-X. Xu, L. Vivien, J. Lapointe, S. Janz, and M. Dado, "Single-etch subwavelength engineered fiber-chip grating couplers for 1.3 μm datacom wavelength band," *Optics express*, vol. 24, no. 12, pp. 12 893–12 904, 2016.

[11] Y. Wang, L. Xu, A. Kumar, Y. Dmello, D. Patel, Z. Xing, R. Li, M. G. Saber, E. El-Fiky, and D. V. Plant, "Compact single-etched sub-wavelength grating couplers for O-band application," *Optics express*, vol. 25, no. 24, pp. 30 582–30 590, 2017.

[12] S. Wang, Y. Hong, Y. Zhu, J. Chen, S. Gao, X. Cai, Y. Shi, and L. Liu, "Compact high-efficiency perfectly-vertical grating coupler on silicon at O-band," *Optics express*, vol. 25, no. 18, pp. 22 032–22 037, 2017.

[13] M. Tokushima, J. Ushida, and K. Kurata, "Folded shallow grating couplers with minimal back reflection and extended coupling bandwidth for robust coupling to multimode fibers," *Journal of Lightwave Technology*, vol. 35, no. 2, pp. 246–257, 2017.

[14] F. Boeuf, S. Cremer, E. Temporiti, M. Fere, M. Shaw, C. Baudot, N. Vulliet, T. Pinguet, A. Mekis, G. Masini *et al.*, "Silicon photonics r&d and manufacturing on 300-mm wafer platform," *Journal of lightwave technology*, vol. 34, no. 2, pp. 286–295, 2016.

[15] A. La Porta, J. Weiss, R. Dangel, D. Jubin, N. Meier, J. Hofrichter, C. Caer, F. Horst, and B. Offrein, "Silicon photonics packaging for highly scalable optical interconnects," in *Electronic Components and Technology Conference (ECTC), 2015 IEEE 65th*. IEEE, 2015, pp. 1299–1304.

[16] N. Mangal, J. Missinne, G. Van Steenberge, J. Van Campenhout, and B. Snyder, "Packaging silicon photonics with polymer waveguides for 3D electro-optical integration," in *Photonics Conference (IPC), 2017 IEEE*. IEEE, 2017, pp. 707–708.

[17] N. Mangal, J. Missinne, G. Roelkens, J. V. Campenhout, G. V. Steenberge, and B. Snyder, "Expanded-beam through-substrate coupling interface for alignment tolerant packaging of silicon photonics," in *2018 Optical Fiber Communications Conference and Exposition (OFC)*. IEEE, 2018, pp. 1–3.

[18] B. Snyder, N. Mangal, G. Lepage, S. Balakrishnan, X. Sun, N. Pantano, M. Rakowski, L. Bogaerts, P. De Heyn, P. Verheyen, A. Miller, M. Pantouvaki, P. Absil, and J. Van Campenhout, "Packaging and assembly challenges for 50G silicon photonics interposers," in *2018 Optical Fiber Communications Conference and Exposition (OFC)*. IEEE, 2018, pp. 1–3.

[19] S. B. Yoo, R. Proietti, and P. Grani, "Photonics in data centers," in *Optical Switching in Next Generation Data Centers*. Springer, 2018, pp. 3–21.

[20] J. Notaros, F. Pavanello, M. T. Wade, C. M. Gentry, A. Atabaki, L. Alloatti, R. J. Ram, and M. A. Popović, "Ultra-efficient CMOS fiber-to-chip grating couplers," in *Optical Fiber Communications Conference and Exhibition (OFC), 2016*. IEEE, 2016, pp. 1–3.

[21] M. T. Wade, F. Pavanello, R. Kumar, C. M. Gentry, A. Atabaki, R. Ram, V. Stojanović, and M. A. Popović, "75% efficient wide bandwidth grating couplers in a 45 nm microelectronics CMOS process," in *Optical Interconnects Conference (OI), 2015 IEEE*. IEEE, 2015, pp. 46–47.

[22] W. S. Zaoui, M. F. Rosa, W. Vogel, M. Berroth, J. Butschke, and F. Letzkus, "Cost-effective CMOS-compatible grating couplers with backside metal mirror and 69% coupling efficiency," *Optics express*, vol. 20, no. 26, pp. B238–B243, 2012.

[23] C. Kopp, E. Augendre, R. Orobtchouk, O. Lemonnier, and J.-M. Fedeli, "Enhanced fiber grating coupler integrated by wafer-to-wafer bonding," *Journal of Lightwave Technology*, vol. 29, no. 12, pp. 1847–1851, 2011.

[24] S. K. Selvaraja, D. Vermeulen, M. Schaekers, E. Sleeckx, W. Bogaerts, G. Roelkens, P. Dumon, D. Van Thourhout, and R. Baets, "Highly efficient grating coupler between optical fiber and silicon photonic circuit," in *Conference on Lasers and Electro-Optics*. Optical Society of America, 2009, p. CTuC6.

[25] N. Mangal, J. Missinne, J. Van Campenhout, G. Van Steenberge, and B. Snyder, "Integration of ball lens in through-package via to enable photonic chip-to-board coupling," in *2018 IEEE 68th Electronic Components and Technology Conference (ECTC)*. IEEE, 2018, pp. 1140–1145.

[26] T. Tamir and S.-T. Peng, "Analysis and design of grating couplers," *Applied physics*, vol. 14, no. 3, pp. 235–254, 1977.

[27] E. Bosman, J. Missinne, B. Van Hoe, G. Van Steenberge, S. Kalathimekkad, J. Van Erps, I. Milenkov, K. Panajotov, T. Van Gijseghem, P. Dubruel, H. Thienpont, and P. Van Daele, "Ultrathin optoelectronic device packaging in flexible carriers," *IEEE Journal of selected topics in quantum electronics*, vol. 17, no. 3, pp. 617–628, 2011.

[28] A. Rahim, E. Ryckeboer, A. Z. Subramanian, S. Clemmen, B. Kuyken, A. Dhakal, A. Raza, A. Hermans, M. Muneeb, S. Dhoore, Y. Li, U. Dave, P. Bienstman, N. Le Thomas, G. Roelkens, D. Van Thourhout, P. Helin, S. Severi, X. Rottenberg, and R. Baets, "Expanding the silicon photonics portfolio with silicon nitride photonic integrated circuits," *Journal of Lightwave Technology*, vol. 35, no. 4, pp. 639–649, 2017.

[29] S. Romero-García, F. Merget, F. Zhong, H. Finkelstein, and J. Witzens, "Visible wavelength silicon nitride focusing grating coupler with AlCu/TiN reflector," *Optics letters*, vol. 38, no. 14, pp. 2521–2523, 2013.

[30] F. Van Laere, G. Roelkens, M. Ayre, J. Schrauwen, D. Taillaert, D. Van Thourhout, T. F. Krauss, and R. Baets, "Compact and highly efficient grating couplers between optical fiber and nanophotonic waveguides," *Journal of lightwave technology*, vol. 25, no. 1, pp. 151–156, 2007.

[31] Z. Nong, Y. Luo, S. Gao, H. Huang, S. Yu, and X. Cai, "Low-loss two-dimensional grating coupler on SOI platform with bonded metal mirror," in *CLEO: QELS_Fundamental Science*. Optical Society of America, 2017, pp. JW2A–143.

[32] Y. Ding, C. Peucheret, H. Ou, and K. Yvind, "Fully etched apodized grating coupler on the SOI platform with -0.58 db coupling efficiency," *Optics letters*, vol. 39, no. 18, pp. 5348–5350, 2014.

[33] P. Johnson and R. Christy, "Optical constants of transition metals: Ti, V, Cr, Mn, Fe, Co, Ni, and Pd," *Physical Review B*, vol. 9, no. 12, p. 5056, 1974.

[34] C. Kopp, S. Bernabe, B. B. Bakir, J.-M. Fedeli, R. Orobtchouk, F. Schrank, H. Porte, L. Zimmermann, and T. Tekin, "Silicon photonic circuits: on-CMOS integration, fiber optical coupling, and packaging," *IEEE Journal of Selected Topics in Quantum Electronics*, vol. 17, no. 3, pp. 498–509, 2011.